Research Article

Numerical simulation of MHD flow and heat transfer inside T-shaped cavity by the parallel walls motion

A. A. El Desouky[1] · Hassan Nasr Ahamed Ismail[1] · Aly Maher Abourabia[2] · Nasrelden A. Ahmed[1]

Received: 31 December 2019 / Accepted: 27 February 2020 / Published online: 14 March 2020

Abstract
In this paper, the heat and mass transfer due to the steady, laminar, and incompressible MHD flow inside T-shaped cavity is numerically calculated. The fluid moves under an external magnetic field applied to the vertical axis of the cavity, and the cavity is driven by the parallel horizontal velocities from the upper and lower parts of the cavity. The governing equations of continuity, momentum, and the energy are solved simultaneously by using the finite difference method. The effect of Reynolds and Hartmann numbers on the streamlines, vorticity, temperature distribution, and velocity vectors in *x*–*y* directions is simulated. According to the motion of the fluid inside the cavity, some vertices vorticity will appear. It observes of their positions and the change in its positions under changing the Reynolds and Hartmann numbers. The results are presented in graphs and tables.

Keywords Magnetohydrodynamics · Heat and mass transfer · T-shaped cavity · Finite difference method

List of symbols

B_0	External magnetic field (Tesla (T))
Ec	Eckert number
C_P	Specific heat at constant pressure $\left(\mathrm{J\ kg^{-1}\ K^{-1}}\right)$
Ha	Hartmann number
k	Thermal conductivity $\left(\mathrm{W\,m^{-1}\,K^{-1}}\right)$
L	Length of the cavity (m)
P	Fluid pressure (Pa or N $\mathrm{m^{-2}}$)
Pr	Prandtl number
Re	Reynolds number
T	Fluid temperature (K)
T_c	Low wall temperature (K)
T_h	High wall temperature (K)
U	Horizontal fluid velocity $\left(\mathrm{m\,s^{-1}}\right)$
u	Dimensionless horizontal velocity
u_0	Characteristic velocity
V	Vertical fluid velocity $\left(\mathrm{m\,s^{-1}}\right)$
v	Dimensionless vertical velocity
X, Y	Cartesian coordinates (m)
x, y	Dimensionless Cartesian coordinates

Greek symbols

ρ	Fluid density (kg $\mathrm{m^{-3}}$)
σ	Electrical conductivity ($\Omega^{-1}\ \mathrm{m^{-1}}$)
μ	Fluid viscosity (Pa s)
θ	Dimensionless temperature
ψ^*	Stream function ($\mathrm{m^2\ s^{-1}}$)
ψ	Dimensionless stream function
ω^*	Vorticity function ($\mathrm{s^{-1}}$)
ω	Dimensionless vorticity function

✉ A. A. El Desouky, ahmed.mohammed@bhit.bu.edu.eg; Hassan Nasr Ahamed Ismail, hassan.ismaeel@bhit.bu.edu.eg; Aly Maher Abourabia, aly.abourabia@science.menofia.edu.eg; Nasrelden A. Ahmed, Nasereldein.ahmed@bhit.bu.edu.eg | [1]Basic Engineering Sciences Department, Benha Faculty of Engineering, Benha University, Benha 13512, Egypt. [2]Mathematics Department, Faculty of Science, Menoufia University, Shebin Elkom 32511, Egypt.

SN Applied Sciences (2020) 2:654 | https://doi.org/10.1007/s42452-020-2371-6

1 Introduction

The heat and mass transfer inside various shaped cavities is natural phenomenon, and it is known in engineering and has been the topic of many research engineering studies because of their occurrences and appearances in the various fields used in industrial applications like solar collectors, heat exchangers, electronic chips, and green buildings. Ismail et al. [1, 2] studied numerically the heat and mass transfer of the laminar, incompressible, steady, and viscous fluid inside the T-shaped cavity using a finite difference approximation. They assume the fluid flow is driven from the upper and lower walls once, and from upper wall another once. Sahi et al. [3] investigated numerically the magnetic field effect on the 2-D natural convection inside T-shaped cavity subjected to isothermal boundary conditions using the finite volume method. They investigated the free convective heat transfer due to the temperature difference between the upper cold flat wall and the bottom hot wall. In [4, 5], they studied numerically the mixed convection heat transfer of nanofluids inside a T-shaped lid-driven by finite element method. The nanofluids are considered in the cavity to augment the heat transfer rate such that the upper boundaries have low temperature but the bottom boundaries have high temperature. Esfe et al. [6] investigated numerically the natural convection of fluid flow and heat transfer inside T-shaped cavity filled with nanofluids by using finite volume method, they assumed that the cavity having six walls with high constant temperature and the horizontal top wall with low constant temperature but the bottom wall is kept thermally insulated. Almeshaal et al. [7] investigated numerically the natural convection of the three-dimensional, unsteady, laminar, and incompressible nanofluid inside the T-shaped cavity using control volume method, they assumed that the left side walls have hot temperature and the right side walls are assumed as cold temperature but the bottom and top walls are kept thermally insulated. Hussain et al. [8] investigated numerically the mixed convection and entropy generation rate inside T-shaped porous cavity that filled with nanofluid using finite element method, they assumed that the upper wall has low temperature and the bottom wall is sinusoidally heated, whereas all the other walls are adiabatic. In [9, 10] studied numerically free convection of nanofluid inside ⊥ shaped cavity. Sarkar et al. [11] investigated numerically of MHD mixed convection in a lid-driven rectangular cavities with the wall wavy at the top and rectangular heaters at the bottom wall using finite element method, they assumed that the top of the cavity is driven by a wavy wall with low temperature, while the lower wall has three rectangular heaters with high temperature. Ma et al. [12–14] investigated numerically of natural convection and mixed convection of nanofluid in a U-shaped cavity in the presence of a magnetic field using lattice Boltzmann method (LBM). Selimefendigil and Öztop [15] investigated numerically of mixed convective nanofluid flow in an inclined L-shaped cavity by using the finite element method, they assumed that the cavity is driven from the upper wall with constant velocity, also the left and right walls are considered at high and low temperatures respectively, while the top and bottom walls are adiabatic. Sheremet et al. [16] investigated numerically of the mixed convection flow and heat transfer for micropolar fluid inside triangular cavity using finite element method, they assumed that the cavity is driven from the bottom wall with constant velocity and high-temperature wall, while the left and right walls are considered at low temperature. Ismail et al. [17] investigated numerically heat and mass transfer due to the steady, laminar, and incompressible MHD micropolar fluid flow in a rectangular duct with the slip flow and convective boundary conditions. Haq et al. [18] investigated numerically for heat transfer analysis of water functionalized Fe_3O_4 ferrofluid is performed along with the irreversibility process along a porous semi-annulus. Haq et al. [19] investigated numerically for thermal management of water-based single-wall carbon nanotubes (SWCNTs) inside the partially heated triangular cavity with heated cylindrical obstacle. Haq et al. [20] investigated numerically for heat transfer analysis is performed for Magnetohydrodynamic (MHD) water-based single-wall carbon nanotubes (SWCNTs) inside a C-shaped cavity that is partially heated along the left vertical wall in the presence of magnetic field. Haq et al. [21] investigated numerically for natural convection flow in a partially heated trapezoidal cavity containing non-Newtonian Casson fluid. A non-Newtonian model of Casson fluid is used to develop the governing flow equations.

Our effort in this paper is dedicated to study the heat and mass transfer inside a T-shaped cavity with two parallel walls in motion from the top and bottom walls under the effect of the external magnetic field.

2 Mathematical formulation

2.1 Physical description

Consider the steady, laminar, and incompressible viscous fluid is moved inside a T-shaped cavity under transverse external magnetic flux density (B_0) applied in Y-direction as shown in Fig. 1a. The cavity has a length (L) and can be divided into two parts, the upper part is called the head with length L and height ($0.4L$), while the lower part is called the tail with length ($0.4L$) and hight ($0.6L$) as in Fig. 1a. The upper and the lower walls are moving with

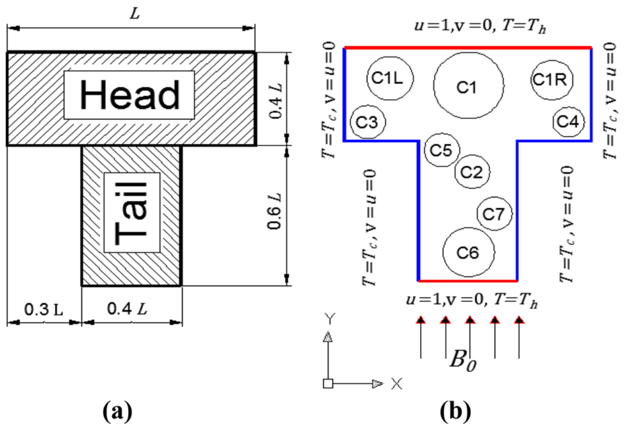

Fig. 1 **a** Statement for T-shaped cavity, **b** the dimension of the cavity

uniform horizontal velocity in X-direction ($U = u_0$) and are maintained at high temperature ($T = T_h$), while the other walls are maintained at low temperature ($T = T_c$). Figure 1b presents the locations of the vertices inside the cavity that formed due to the horizontal velocities and magnetic field effect. In this cavity, the upper and lower horizontal velocities are caused to form the primary and secondary primary vertices (C1) and (C6), respectively, that leads to form the secondary vertices (C3, C4, and C2) and tertiary vertices (C5 and C7). When the velocity is decreased, the primary vertex (C1) is divided into (C1L and C1R).

2.2 Mathematical modeling

Assume the working fluid to be incompressible, electrically conducting, and Newtonian fluid. Two-dimensional MHD equations have been applied to the cavity. The flow of the fluid is assumed laminar and steady state with constant fluid properties. The fluid is movement inside the cavity under transverse external magnetic flux density (B_0) applied in Y-direction. Assume the walls are electrically insulated, so that it neglects the electrical field (E), and the magnetic permeability (μ_0) of the fluid is low (low magnetic Reynolds number) so that it can neglect the induced magnetic field.

According to the assumptions stated above, the MHD equations that contain continuity, momentum, and energy [1, 2] under the effect of magnetic field for the present cavity can be written as:

$$\frac{\partial U}{\partial X} + \frac{\partial V}{\partial Y} = 0 \tag{1}$$

$$\rho\left(U\frac{\partial U}{\partial X} + V\frac{\partial U}{\partial Y}\right) = -\frac{\partial P}{\partial X} + \mu\left(\frac{\partial^2 U}{\partial X^2} + \frac{\partial^2 U}{\partial Y^2}\right) - \sigma U B_0^2 \tag{2}$$

$$\rho\left(U\frac{\partial V}{\partial X} + V\frac{\partial V}{\partial Y}\right) = -\frac{\partial P}{\partial Y} + \mu\left(\frac{\partial^2 V}{\partial X^2} + \frac{\partial^2 V}{\partial Y^2}\right) \tag{3}$$

$$\rho C_P\left(U\frac{\partial T}{\partial X} + V\frac{\partial T}{\partial Y}\right) = k\left(\frac{\partial^2 T}{\partial X^2} + \frac{\partial^2 T}{\partial Y^2}\right) + \sigma U^2 B_0^2 \tag{4}$$

The boundary conditions are classified as follows.

On the top and bottom walls ($U = 1$, $V = 0$, $T = T_h$), while on other walls ($U = V = 0$, $T = T_C$).

Convenient the horizontal and velocities into the stream function and vorticity forms where;

$$U = \frac{\partial \psi^*}{\partial Y}, \quad V = -\frac{\partial \psi^*}{\partial X}, \quad \omega^* = \left(\frac{\partial V}{\partial X} - \frac{\partial U}{\partial Y}\right). \tag{5}$$

Applying the stream function and vorticity equation into governing equations we get;

$$\omega^* = -\left(\frac{\partial^2 \psi^*}{\partial X^2} + \frac{\partial^2 \psi^*}{\partial Y^2}\right) \tag{6}$$

$$\rho\left(\frac{\partial \psi^*}{\partial Y}\frac{\partial \omega^*}{\partial X} - \frac{\partial \psi^*}{\partial X}\frac{\partial \omega^*}{\partial Y}\right) = \mu\left[\frac{\partial^2 \omega^*}{\partial X^2} + \frac{\partial^2 \omega^*}{\partial Y^2}\right] + \sigma B_0^2 \frac{\partial^2 \psi^*}{\partial Y^2} \tag{7}$$

$$\rho C_P\left(\frac{\partial \psi^*}{\partial Y}\frac{\partial T}{\partial X} - \frac{\partial \psi^*}{\partial X}\frac{\partial T}{\partial Y}\right) = k\left[\frac{\partial^2 T}{\partial X^2} + \frac{\partial^2 T}{\partial Y^2}\right] + \sigma B_0^2 \left(\frac{\partial \psi^*}{\partial Y}\right)^2 \tag{8}$$

It is convenient the governing equations into non-dimensional forms by using the scale parameters as following;

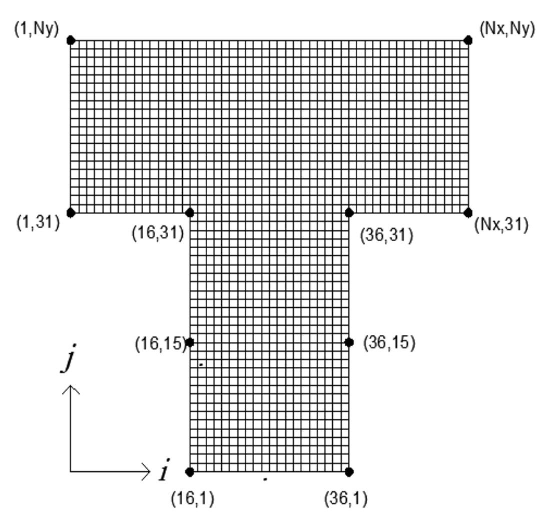

Fig. 2 Grid generation for T-shaped cavity

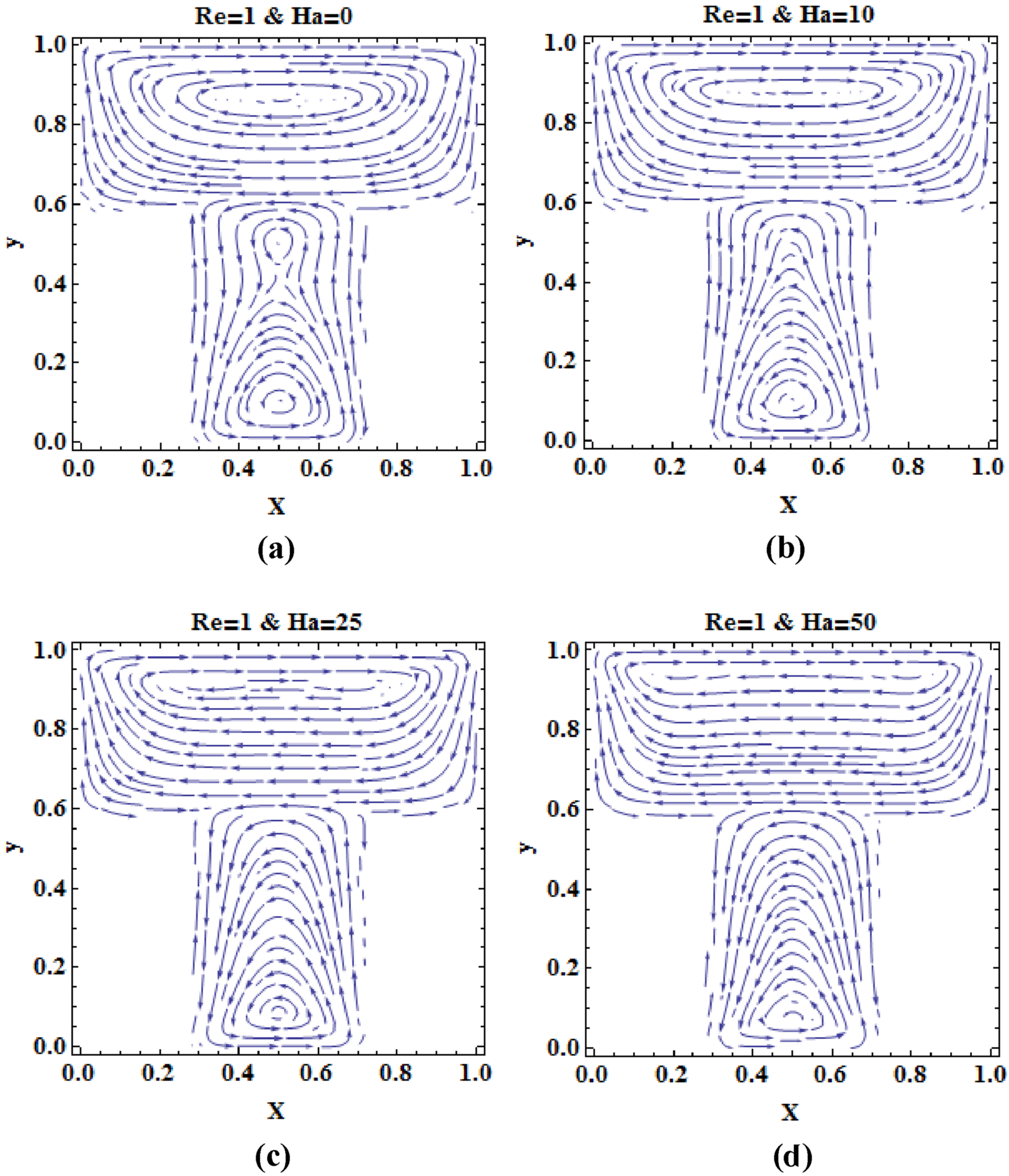

Fig. 3 The velocity vector profile at Re = 1 and **a** Ha = 0, **b** Ha = 10, **c** Ha = 25, **d** Ha = 50

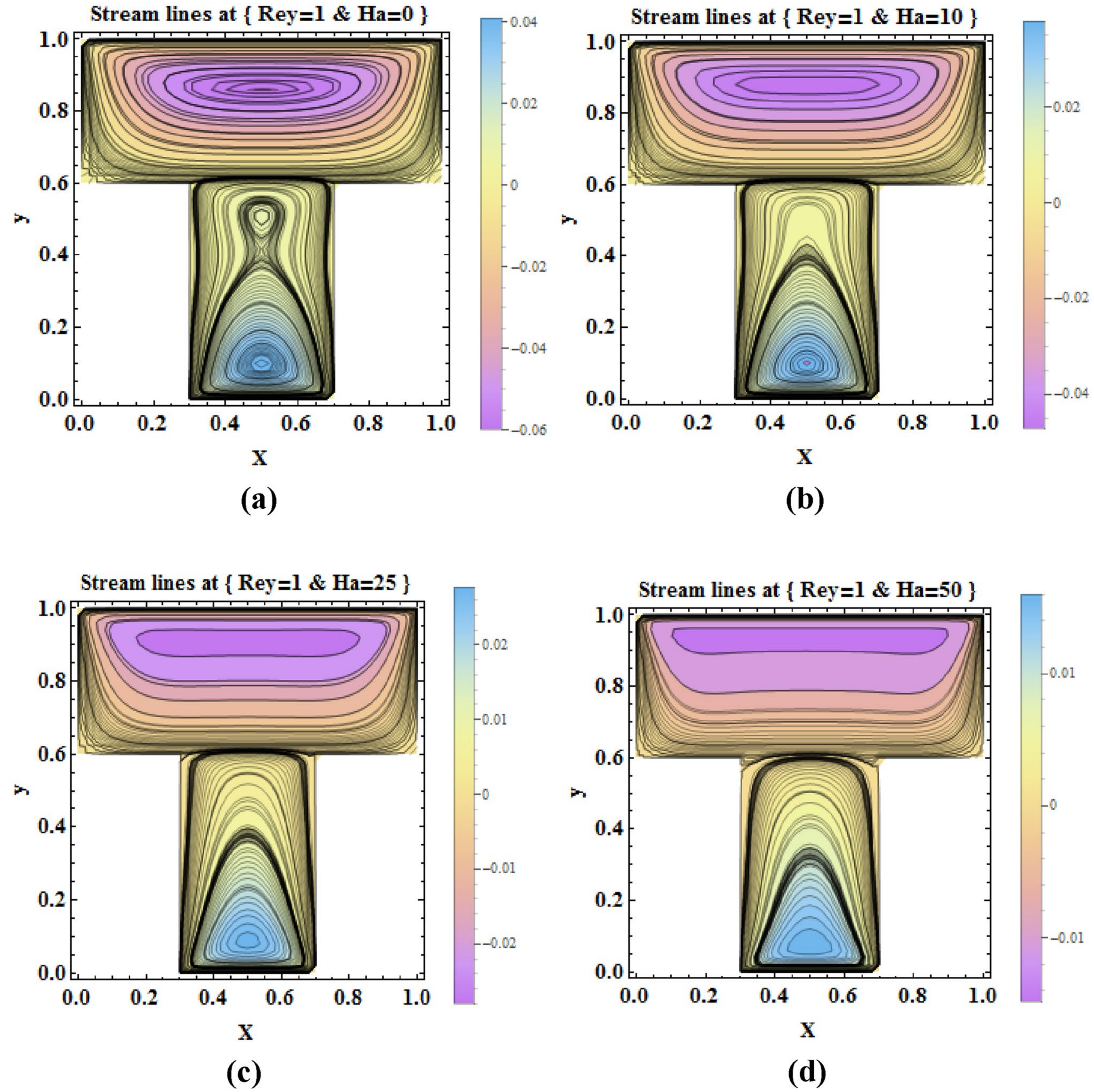

Fig. 4 The streamlines profile at Re = 1 and **a** Ha = 0, **b** Ha = 10, **c** Ha = 25, **d** Ha = 50

$$(x, y) = \frac{(X, Y)}{L}, \quad (u, v) = \frac{(U, V)}{u_0},$$
$$\psi = \frac{\psi^*}{u_0 L}, \quad \omega = \frac{\omega^* L}{u_0}, \quad \theta = \frac{T - T_c}{T_h - T_c} \tag{9}$$

By applying the scale parameters into Eqs. (6–8), we get;

$$\omega = -\left(\frac{\partial^2 \psi}{\partial x^2} + \frac{\partial^2 \psi}{\partial y^2}\right) \tag{10}$$

$$\left(\frac{\partial \psi}{\partial y}\frac{\partial \omega}{\partial x} - \frac{\partial \psi}{\partial x}\frac{\partial \omega}{\partial y}\right) = \frac{1}{\mathrm{Re}}\left[\frac{\partial^2 \omega}{\partial x^2} + \frac{\partial^2 \omega}{\partial y^2}\right] + \frac{\mathrm{Ha}^2}{\mathrm{Re}}\frac{\partial^2 \psi}{\partial y^2} \tag{11}$$

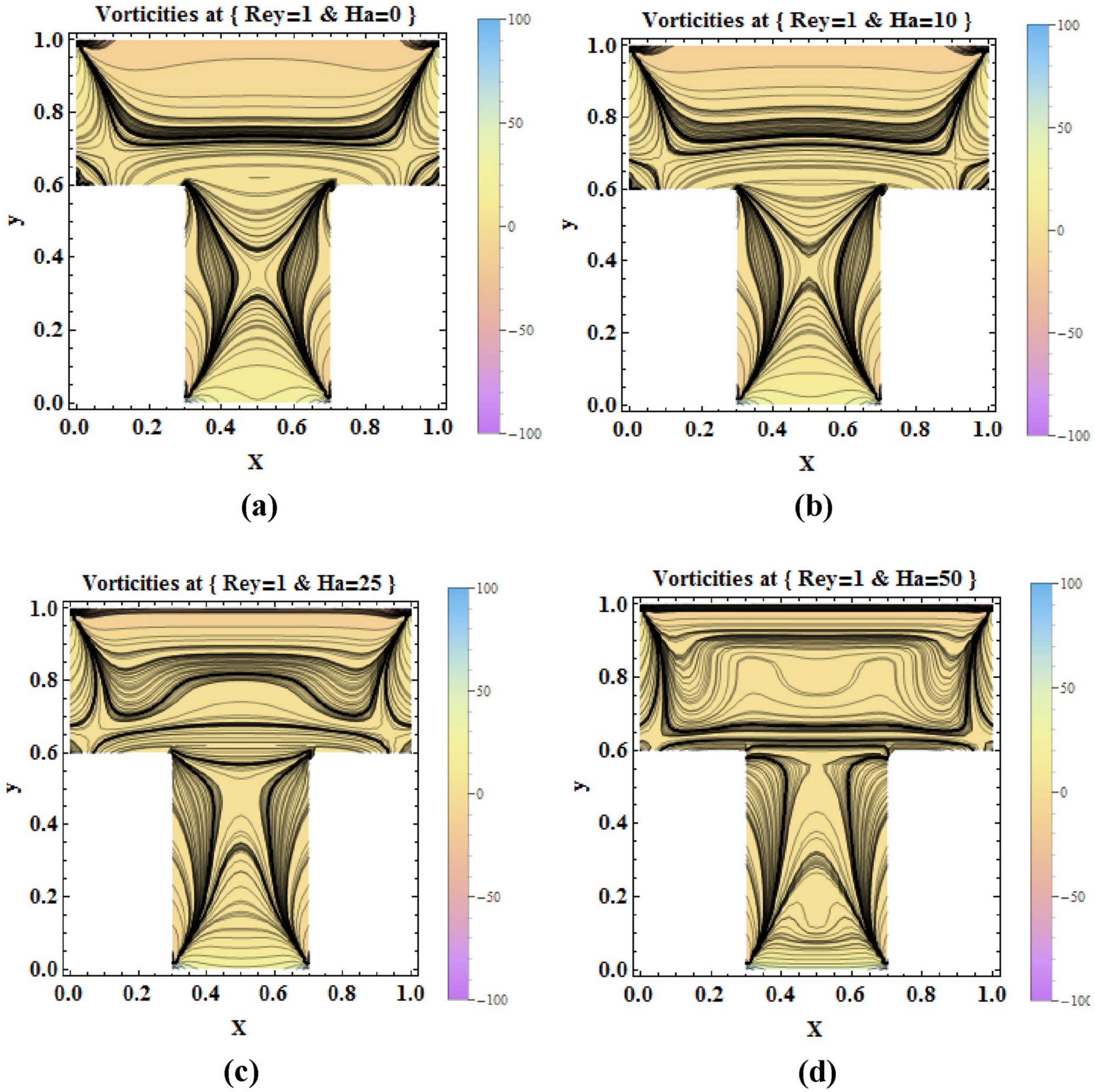

Fig. 5 The vorticity profile at Re = 1 and **a** Ha = 0, **b** Ha = 10, **c** Ha = 25, **d** Ha = 50

$$\left(\frac{\partial\psi}{\partial y}\frac{\partial\theta}{\partial x}-\frac{\partial\psi}{\partial x}\frac{\partial\theta}{\partial y}\right)=\frac{1}{\mathrm{PrRe}}\left[\frac{\partial^2\theta}{\partial x^2}+\frac{\partial^2\theta}{\partial y^2}\right]+\frac{\mathrm{Ha}^2\mathrm{Ec}}{\mathrm{Re}}\left(\frac{\partial\psi}{\partial y}\right)^2 \tag{12}$$

$$u=\frac{\partial\psi}{\partial y}, v=-\frac{\partial\psi}{\partial x} \tag{13}$$

where Reynolds number ($\mathrm{Re}=\rho u_0 L/\mu$), Hartmann number ($\mathrm{Ha}=B_0 L\sqrt{\sigma/\mu}$), Prandtl number ($\mathrm{Pr}=C_\mathrm{P}\mu/k$), and Eckert number ($\mathrm{Ec}=u_0^2/C_\mathrm{P}(T_\mathrm{h}-T_\mathrm{c})$).

The non-dimensional boundary conditions are classified as follows;

On all horizontal walls $\left(\frac{\partial\psi}{\partial x}=0,\quad \omega=-\frac{\partial^2\psi}{\partial y^2}\right)$, while on all vertical walls $\left(\frac{\partial\psi}{\partial y}=0,\quad \omega=-\frac{\partial^2\psi}{\partial x^2}\right)$.

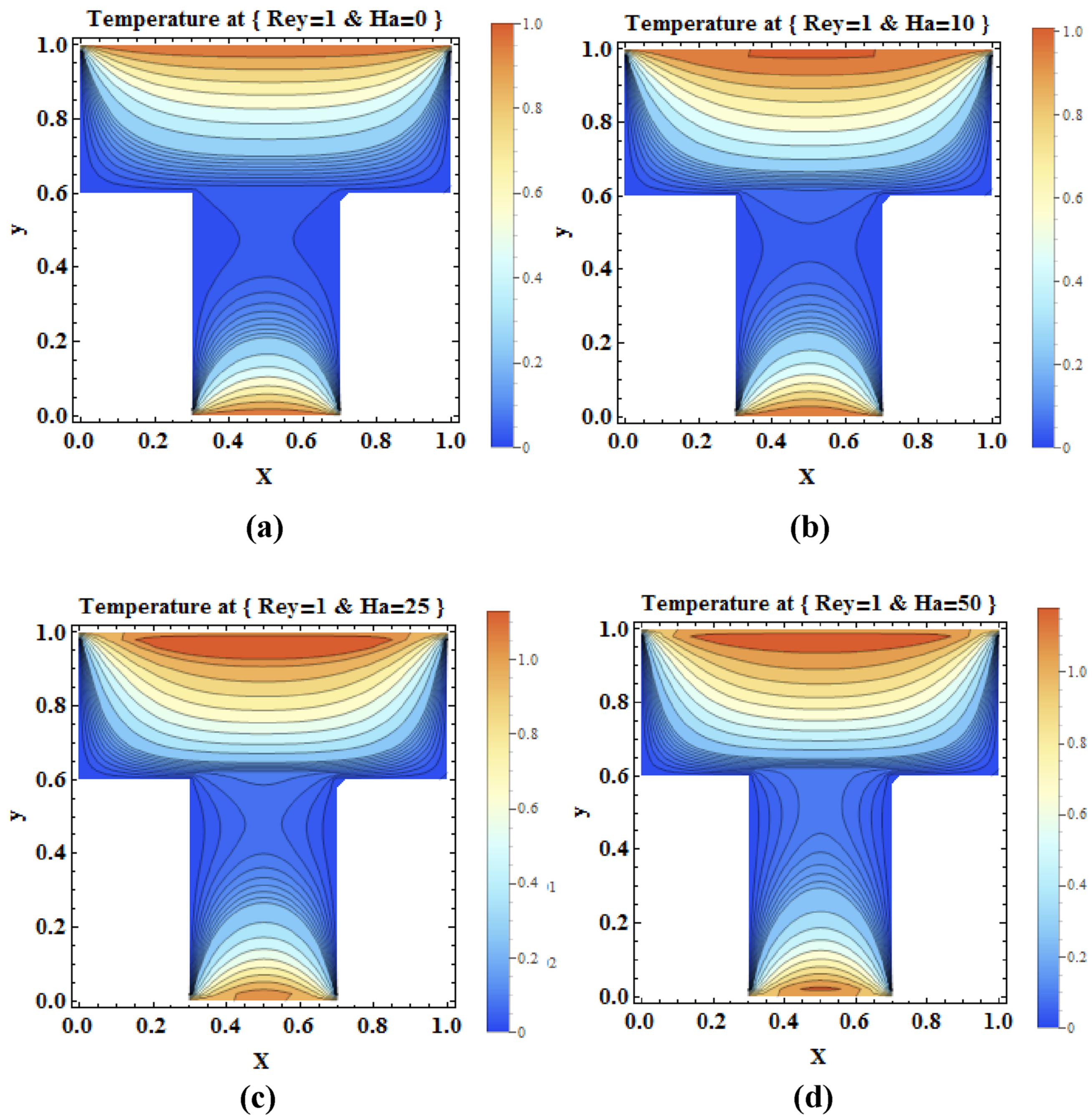

Fig. 6 The temperature profile at Re = 1 and **a** Ha = 0, **b** Ha = 10, **c** Ha = 25, **d** Ha = 50

On the top and bottom walls ($\theta = 1$), while on other walls ($\theta = 0$).
On the top and bottom walls ($u = 1, v = 0$), while on other walls ($u = v = 0$).

3 Results and discussion

In this study, the Magnetohydrodynamic flow and heat transfer for the fluid through T-shaped cavity have been solved numerically by using the finite difference

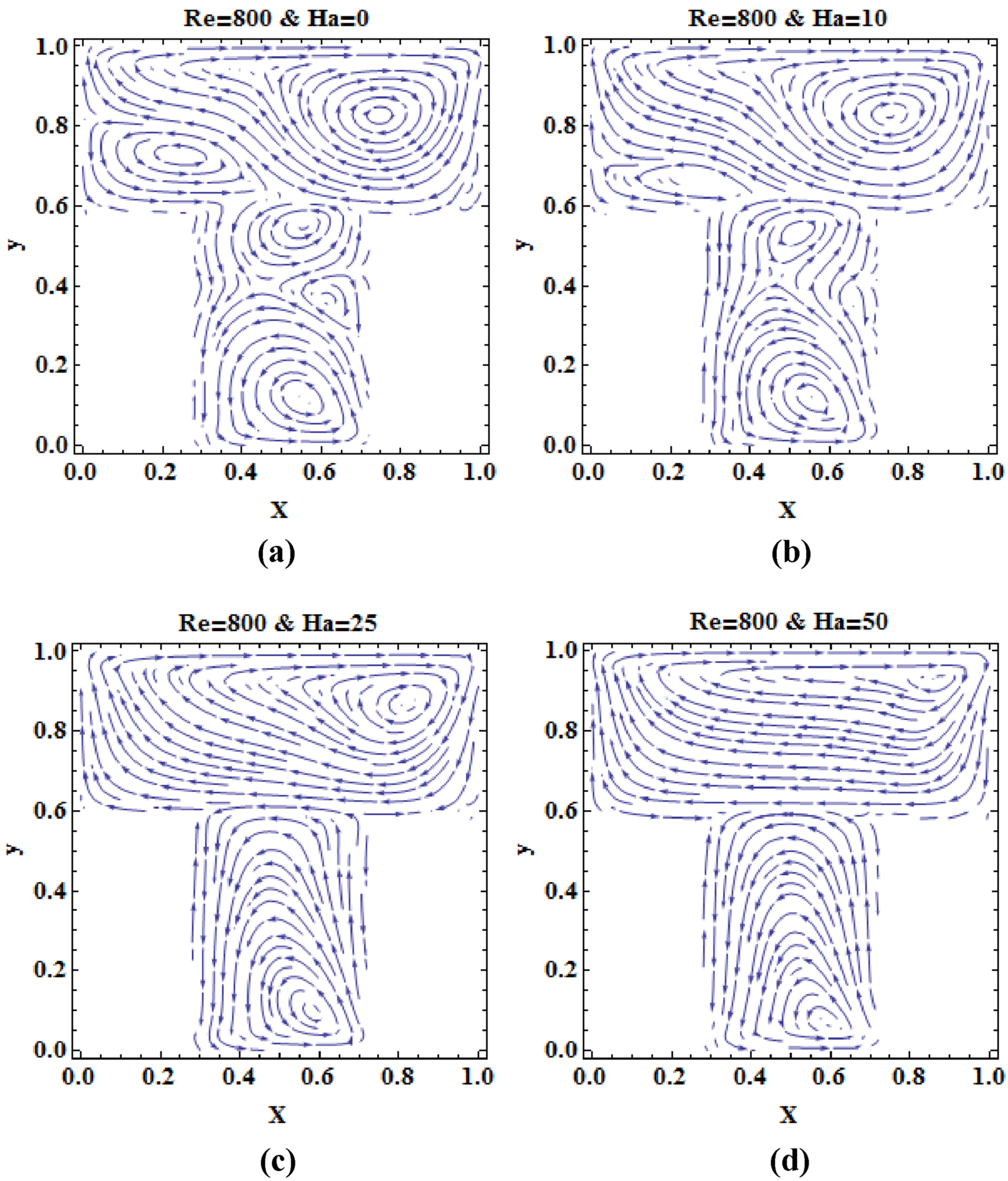

Fig. 7 The velocity vector profile at Re = 800 and **a** Ha = 0, **b** Ha = 10, **c** Ha = 25, **d** Ha = 50

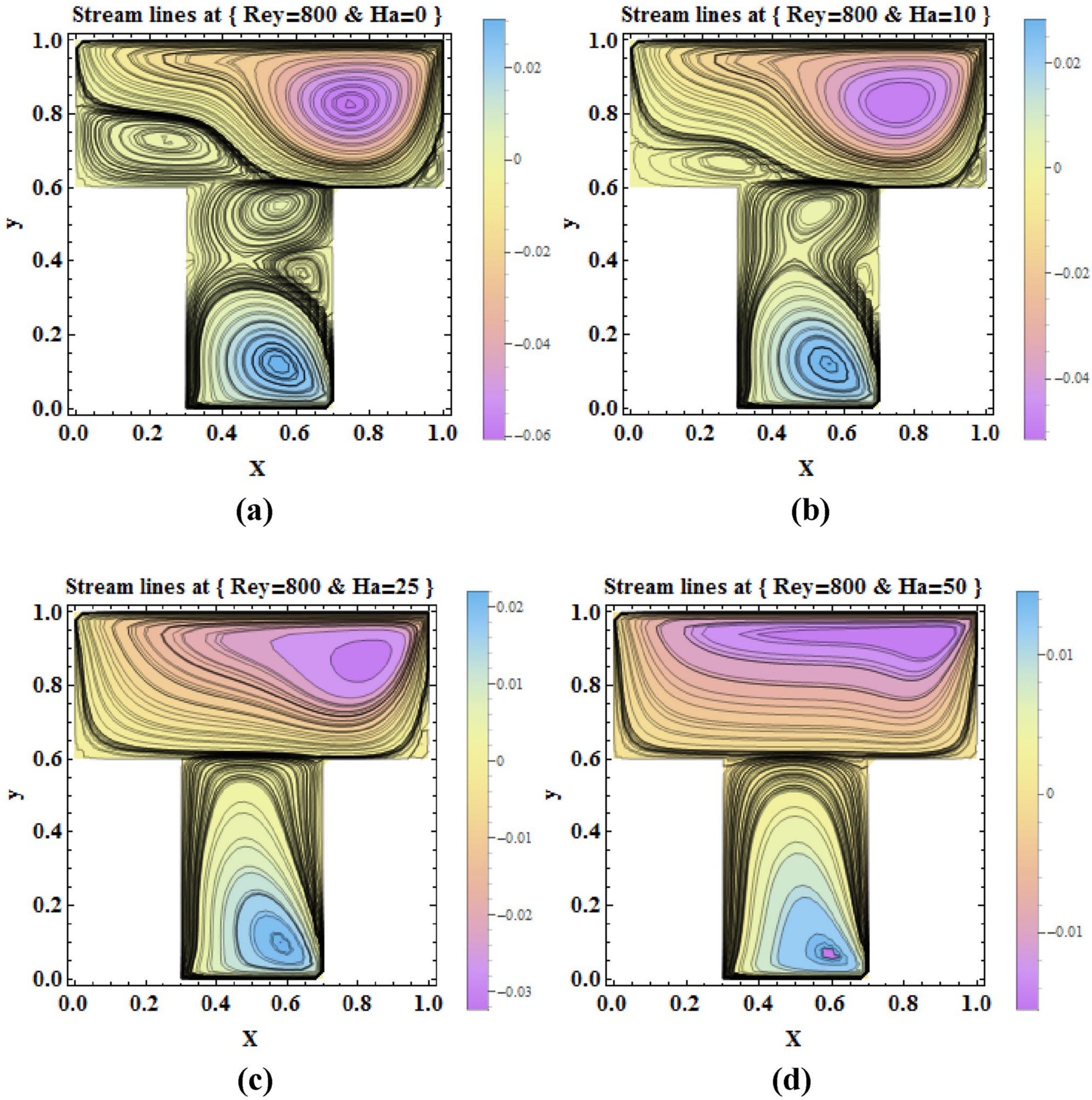

Fig. 8 The streamlines profile at Re = 800 and **a** Ha = 0, **b** Ha = 10, **c** Ha = 25, **d** Ha = 50

approximation with 51 × 51 mesh points [1, 2] where the number of grids $(N_x = 51)$ and $(N_y = 51)$ in (*i* and *j*) directions, respectively, as in Fig. 2.

Using Mathematical software for plotting the velocity vector profiles, streamline profiles, vorticity profiles, and temperature distribution profiles inside the cavity. The governing equations are approximation at (Pr = 1.69) and (Ec = 1) with various Reynolds and Hartmann numbers (Re = 1, 100, 800, 1200, 2000 and Ha = 0, 10, 25, 50).

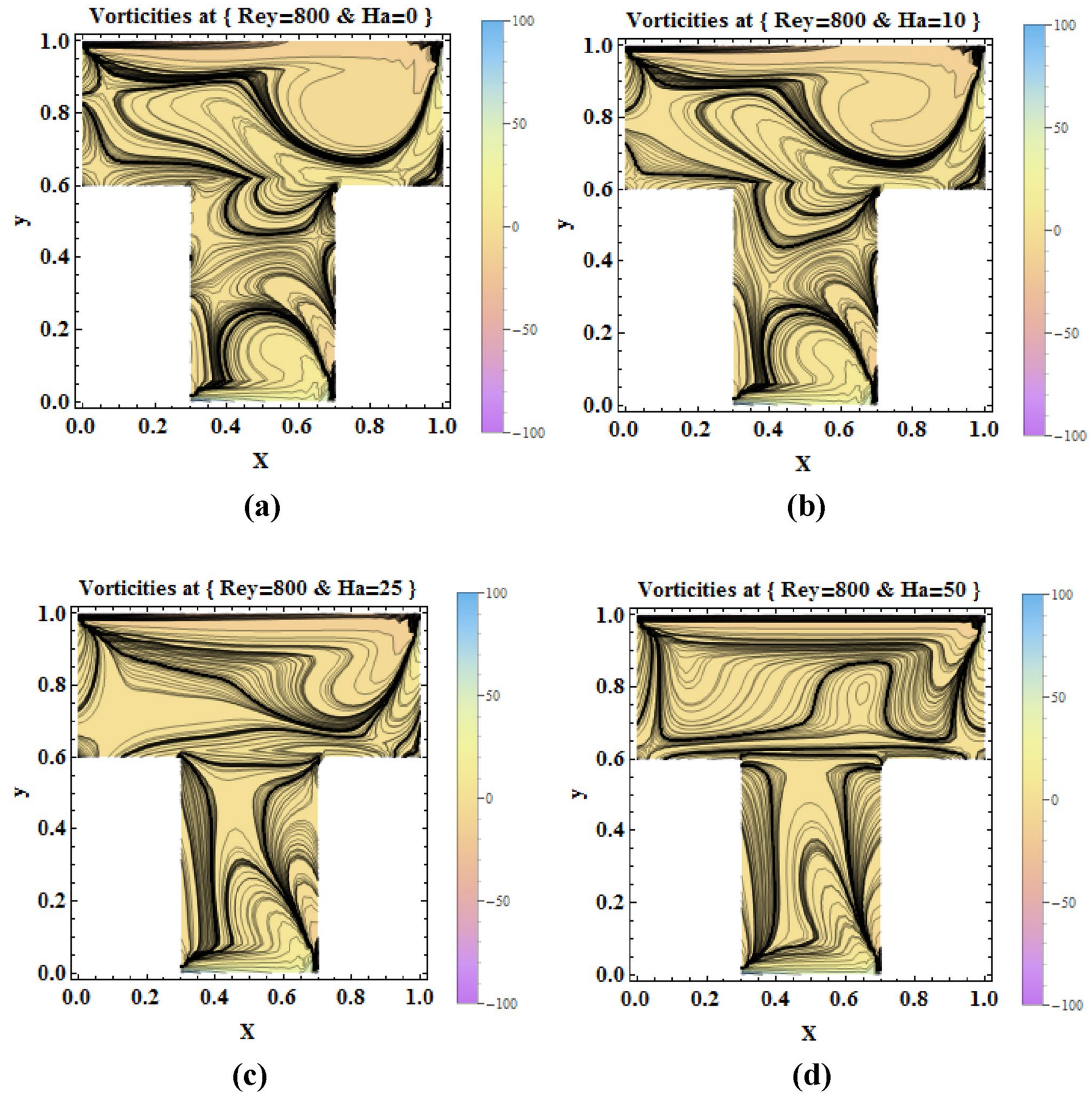

Fig. 9 The vorticity profile at Re = 800 and **a** Ha = 0, **b** Ha = 10, **c** Ha = 25, **d** Ha = 50

Figures 3a and 4a show the dimensionless velocity vector and streamlines profiles at (Re = 1) and (Ha = 0), respectively. It presents the primary vertex (C1) is rotated in clockwise, while the secondary vertices (C2, C3, C4) and secondary primary vertex (C6) are rotated in a counterclockwise direction as in [1]. When Hartmann numbers increase as in Figs. 3b–d and 4b–d, the vertexes (C2, C3 and C4) are hidden and (C1) is divided into two vertices: (C1L) and (C1R). When the Reynolds number increases as in Figs. 7, 8, 11, and 12, other vertexes appear

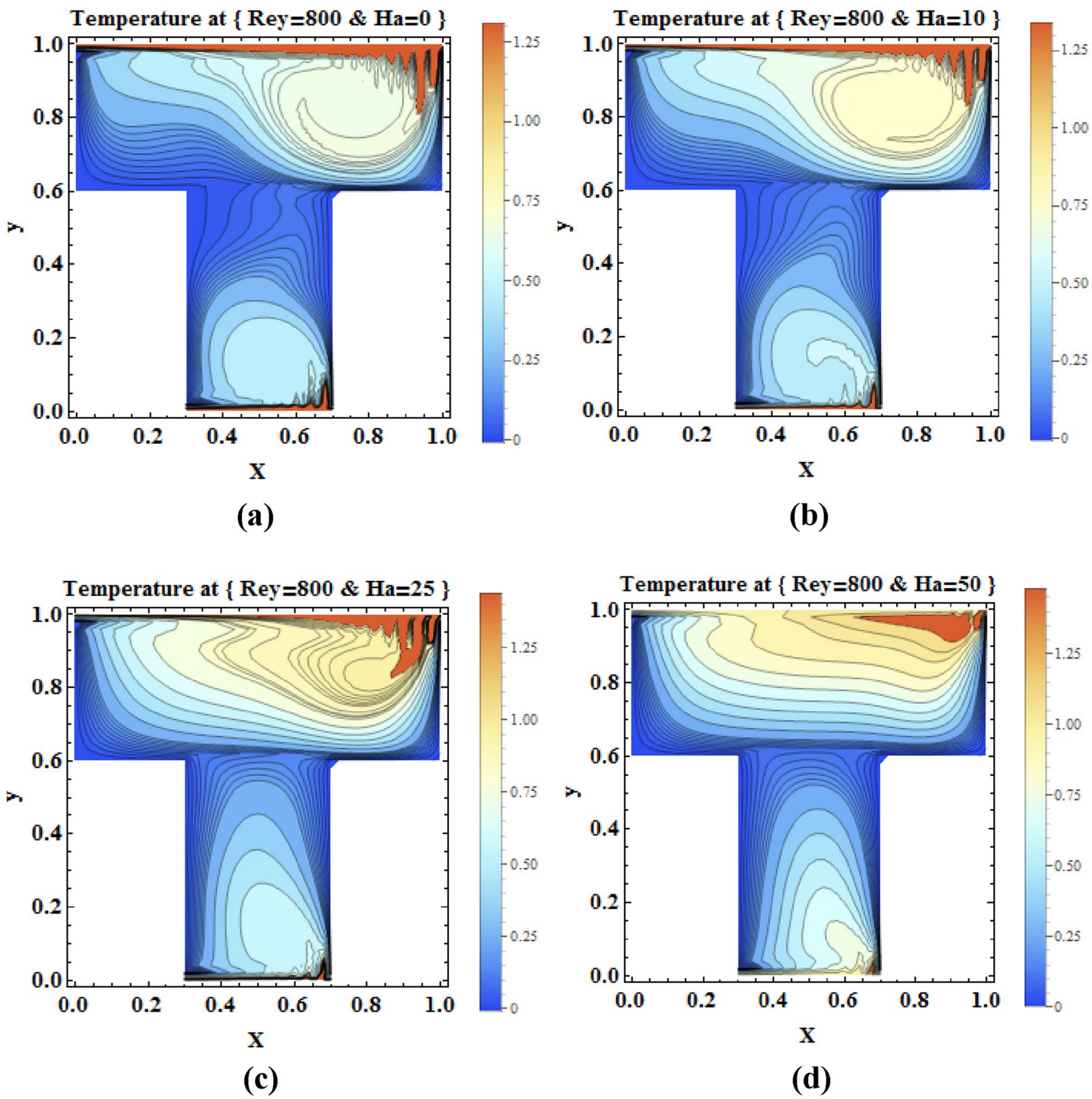

Fig. 10 The temperature profile at Re = 800 and **a** Ha = 0, **b** Ha = 10, **c** Ha = 25, **d** Ha = 50

as the tertiary vertexes (C5andC7) and rotate in clockwise direction. Figures 5, 6, 9, 10, 13, and 14 show the vorticity and temperature profiles at (Re = 1, 800, 2000) and (Ha = 0, 10, 25, 50). It observes the temperature increase with increasing the Reynolds and Hartmann numbers.

Table 1 presents the simulation of primary vertexes (C1, C1L and C1R) at the head part under various Reynolds and Hartmann numbers. It presents the location of the primary vertexes and the stream function. The stream function has a negative sign, this means that the vortices

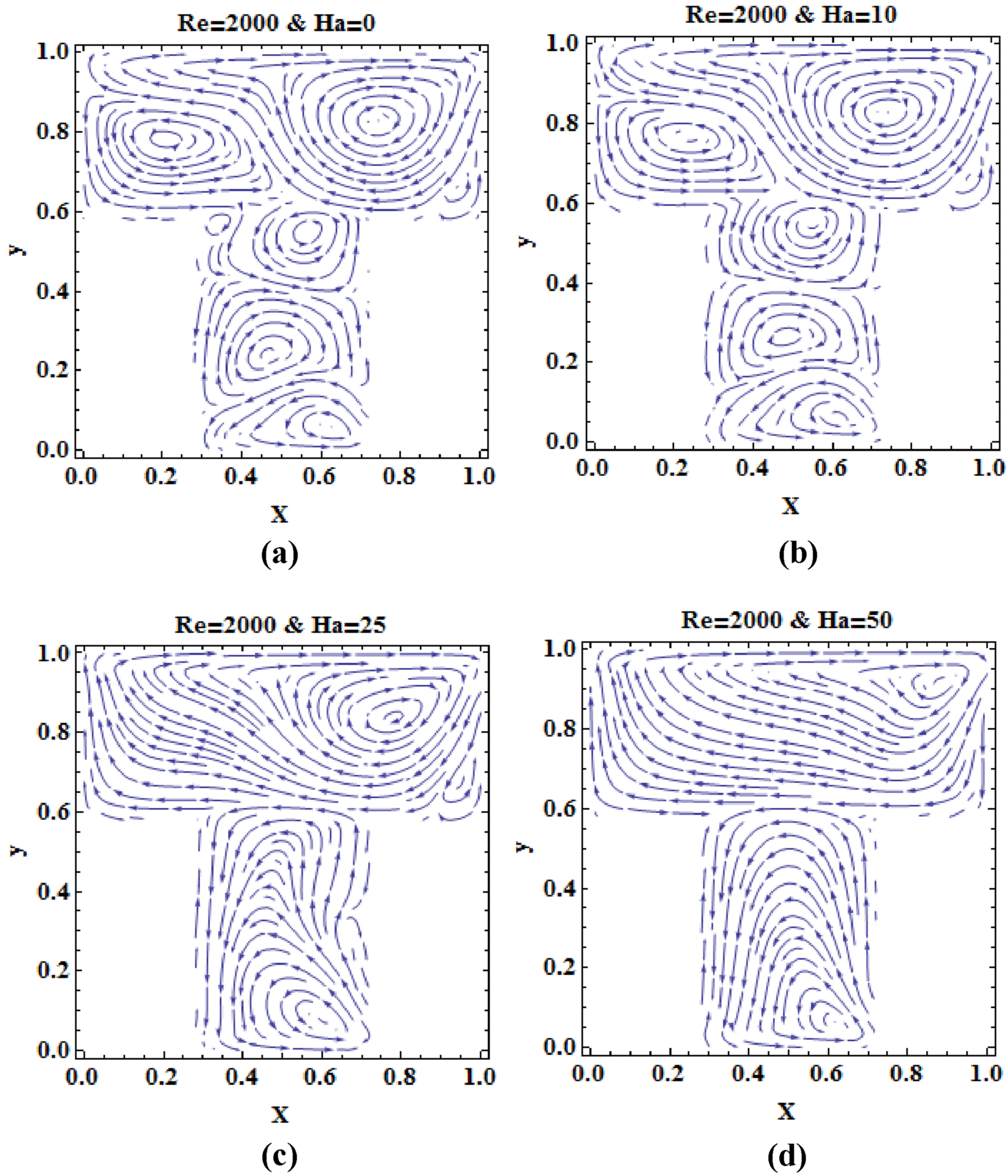

Fig. 11 The velocity vector profile at Re = 2000 and **a** Ha = 0, **b** Ha = 10, **c** Ha = 25, **d** Ha = 50

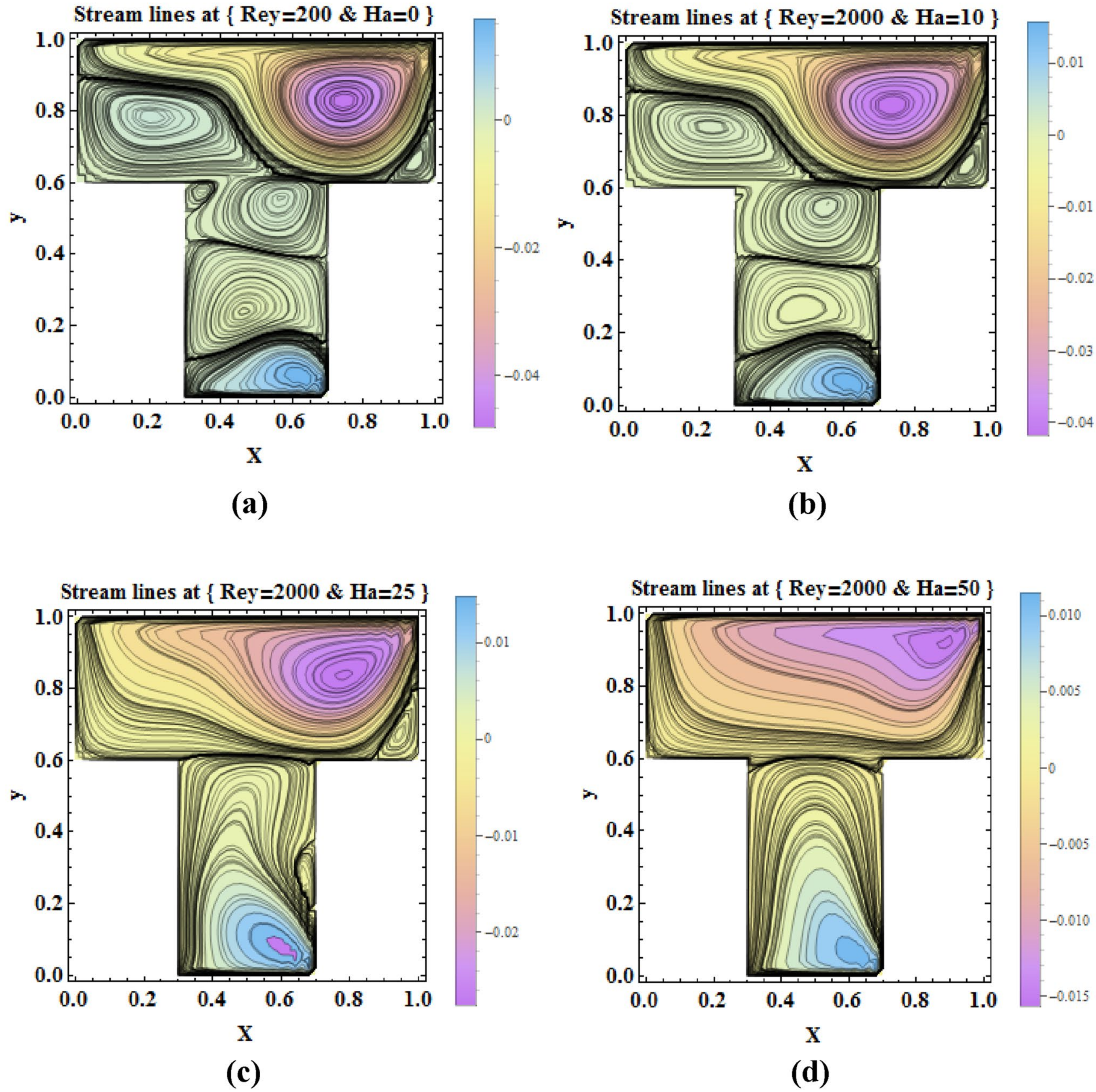

Fig. 12 The streamlines profile at Re = 2000 and **a** Ha = 0, **b** Ha = 10, **c** Ha = 25, **d** Ha = 50

rotating clockwise about *z*-axis as in [1]. Table 2 presents the simulation of secondary vertexes (C3and C4) at the head part under various Reynolds and Hartmann numbers. The stream function in this table has a positive sign, so that the vertexes rotating counterclockwise about *z*-axis. Table 3 presents the simulation of second primary vertex (C6) at the tail part under various Reynolds and Hartmann numbers. The stream function has a positive sign, so that

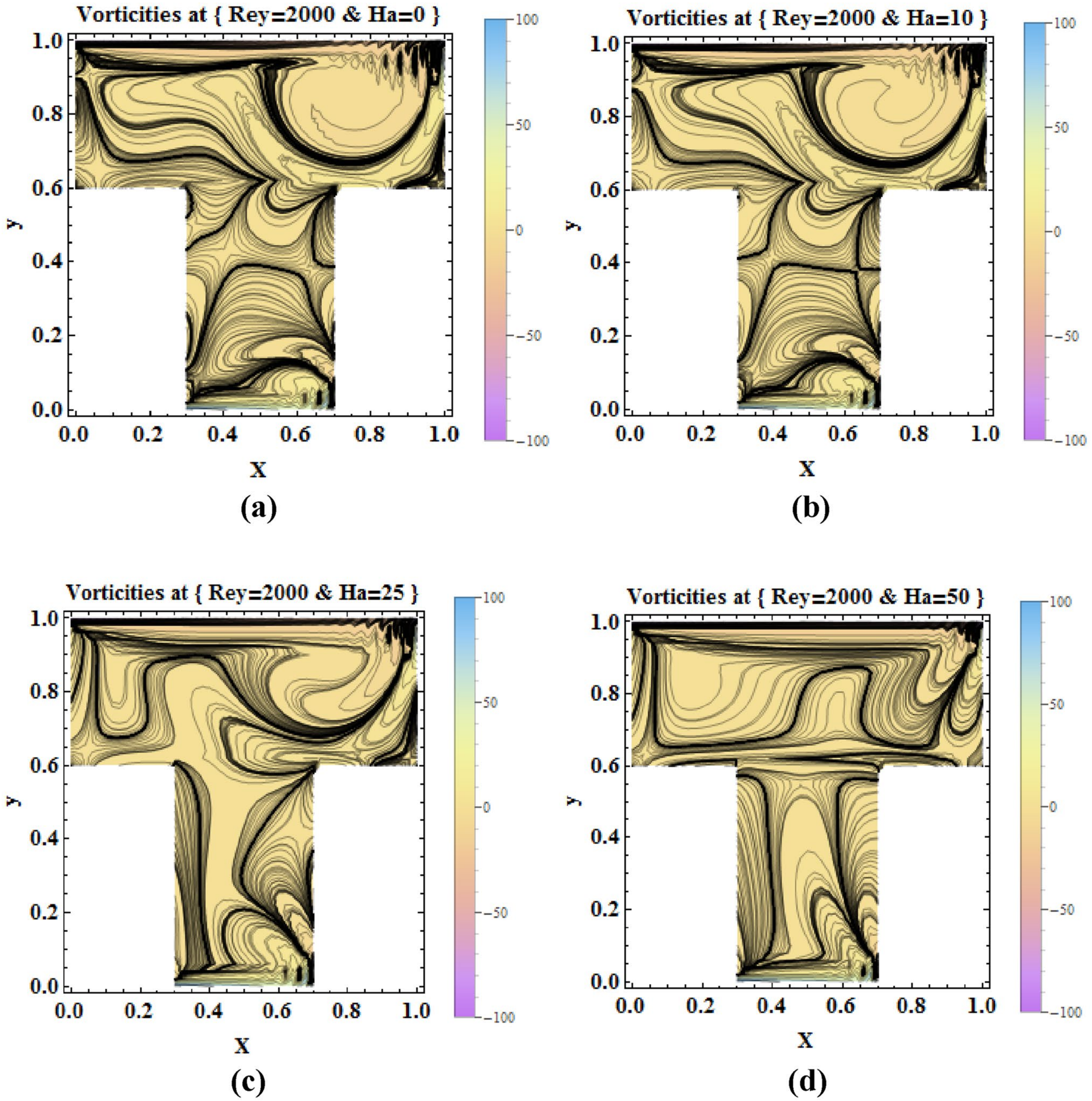

Fig. 13 The vorticity profile at Re = 2000 and **a** Ha = 0, **b** Ha = 10, **c** Ha = 25, **d** Ha = 50

the vortices rotating counterclockwise about *z*-axis. Table 4 presents the simulation of tertiary vertexes (C5) and (C7) at the tail part under various and Hartmann numbers. The stream function has a negative sign, so that the vertexes rotating in clockwise about *z*-axis. Table 5 presents the simulation of secondary vertex (C2) at the tail part under various Reynolds and Hartmann numbers. The stream has a positive sign, this means that the vortices rotating counterclockwise about *z*-axis.

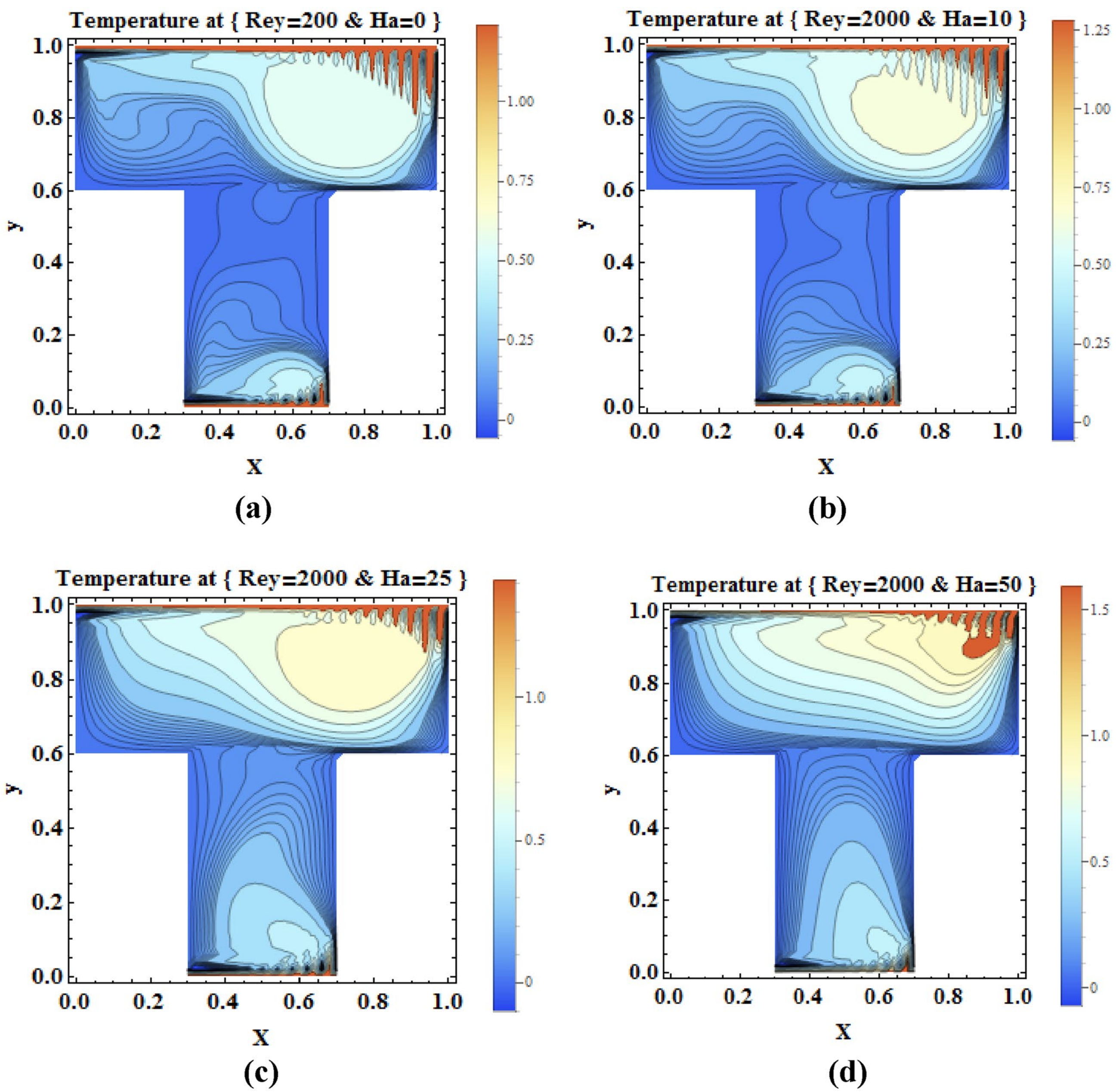

Fig. 14 The temperature profile at Re = 2000 and **a** Ha = 0, **b** Ha = 10, **c** Ha = 25, **d** Ha = 50

4 Conclusion

In this paper, we presented the effects of Reynolds and Hartmann numbers into the mass and heat transfer of steady, laminar and incompressible MHD fluid inside a T-shaped cavity under the effect of the external magnetic field. It assumed the cavity is driven by the two horizontal velocities from the top and bottom walls of the cavity. The results are presented in graphs and tables. Based on the obtained results, we can conclude that:

- When the Reynolds number increases, the locations of vertexes vorticity are changing and increased, also the temperature is increased.
- When the Hartmann number increases, the locations of vertexes vorticity are changing and decreased, also the temperature is increased.

Table 1 Simulation of vertex "C1, C1L and C1R" under the various of Reynolds and Hartmann numbers

Re	Ha	x	y	ψ_{min}	Ha	x	y	ψ_{min}
	C1							
1	0	0.5	0.86	– 0.060328	25	–	–	–
	10	0.48	0.88	– 0.04730159	50	–	–	–
100	0	0.7	0.86	– 0.063144	25	–	–	–
	10	0.72	0.88	– 0.04915645	50	–	–	–
800	0	0.74	0.82	– 0.060781	25	0.82	0.86	−0.032365252657844
	10	0.76	0.82	– 0.05167896	50	0.88	0.94	−0.01556280657
1200	0	0.74	0.82	– 0.055476	25	0.82	0.86	−0.030974080518
	10	0.74	0.82	– 0.04803986	50	0.88	0.92	−0.01586636811
2000	0	0.74	0.82	– 0.047274	25	0.78	0.84	−0.027559501182
	10	0.74	0.82	– 0.04193553	50	0.9	0.92	−0.01571373571
	C1L					*C1R*		
1	25	0.28	0.9	– 0.02802960857	25	0.68	0.9	−0.02805196559
	50	0.2	0.94	– 0.014869998	50	0.8	0.94	−0.014861109364
100	25	0.28	0.92	– 0.02727792423	25	0.76	0.9	−0.02866802385
	50	0.24	0.94	– 0.01477812	50	0.82	0.94	−0.0149543761

Table 2 Simulation of vertex "C3and C4" under the various of Reynolds and Hartmann numbers

Re	Ha	x	y	ψ_{max}	Ha	x	y	ψ_{max}
	C3				C4			
1	0	0.02	0.62	8.72×10^{-6}	0	0.98	0.62	8.74×10^{-6}
	10	0.02	0.62	5.0179×10^{-6}	10	0.98	0.62	5.027×10^{-6}
100	0	0.02	0.62	5.93×10^{-6}	0	0.98	0.62	0.000012
	10	0.02	0.62	2.8239×10^{-6}	10	0.98	0.62	6.473×10^{-6}
800	0	0.24	0.74	0.001581	0	0.96	0.64	0.000187
	10	0.28	0.68	0.000172764	10	0.96	0.64	0.000138301
1200	0	0.22	0.76	0.002789	0	0.96	0.66	0.000433
	10	0.26	0.74	0.0011242538	10	0.96	0.66	0.000378521
2000	0	0.2	0.78	0.003173	0	0.94	0.66	0.000947
	10	0.24	0.76	0.001764773	10	0.94	0.66	0.00083506
	25	–	–	–	25	0.94	0.68	0.00049106493

Table 3 Simulation of vertex "C6" under the various of Reynolds and Hartmann numbers

Re	Ha	x	y	ψ_{max}	Ha	x	y	ψ_{max}
	C6							
1	0	0.5	0.1	0.041065	25	0.5	0.08	0.02765064484
	10	0.5	0.1	0.03789261	50	0.5	0.08	0.015966570549
100	0	0.52	0.1	0.040703	25	0.52	0.08	0.0274808965436
	10	0.52	0.1	0.037614636	50	0.52	0.08	0.0157580937044
800	0	0.56	0.12	0.030533	25	0.58	0.1	0.0221075095736
	10	0.56	0.12	0.02839926	50	0.6	0.06	0.0145884353888
1200	0	0.56	0.1	0.023868	25	0.85	0.1	0.0185536457286
	10	0.56	0.1	0.0229769744	50	0.62	0.06	0.0131091387934
2000	0	0.64	0.06	0.004240	25	0.6	0.08	0.0147585552752
	10	0.64	0.06	0.015747274	50	0.64	0.04	0.0114558563

Table 4 Simulation of vertex "C7and C5" under the various of Reynolds and Hartmann numbers

Re	Ha	x	y	$\psi_{\min}$	Ha	x	y	$\psi_{\min}$
	C7				*C5*			
800	0	0.6	0.36	− 0.000422	0	–	–	–
	10	0.66	0.36	− 0.00012498	10	–	–	–
1200	0	0.48	0.34	− 0.001625	0	0.36	0.56	−0.0000509857
	10	0.6	0.34	− 0.00056838	10	–	–	–
2000	0	0.46	0.24	− 0.001996	0	0.36	0.58	−0.00003545907
	10	0.45	0.26	− 0.00131993	10	–	–	–
	25	0.66	0.28	− 0.00008475807	25	–	–	–

Table 5 Simulation of vertex "C2" under the various of Reynolds and Hartmann numbers

Re	Ha	x	y	$\psi_{\max}$	Re	Ha	x	y	ψ_{max}
	C2								
1	0	0.5	0.5	0.009629	800	25	0.56	0.56	0.002573
	10	–	–	–		50	0.54	0.54	0.02839926
100	0	0.5	0.5	0.008811	1200	25	0.58	0.56	0.001997
	10	0.5	0.44	0.007809407		50	0.54	0.54	0.002175387
2000	0	0.56	0.56	0.001666	2000	10	0.56	0.56	0.001841249

Acknowledgements The authors are grateful to the anonymous referee for his suggestions, which have greatly improved the presentation of the paper.

Authors' contributions The author has made an equal contribution. The author read and approved the final manuscript.

Compliance with ethical standards

Conflict of interest The authors declare that they have no competing interests.

References

1. Ismail HNA, Abourabia AM, Saad AA, El Desouky AA (2015) Numerical simulation for steady incompressible laminar fluid flow and heat transfer inside T-Shaped cavity in the parallel and anti-parallel wall motions. Int J Innov Sci Eng Technol 2:271–280
2. Ismail HNA, Abourabia AM, Saad AA, El Desouky A A (2015) Numerical simulation for steady incompressible laminar fluid flow and heat transfer inside T-shaped cavity using stream function and vorticity. Int J Innov Sci Eng Technol 2:40–48
3. Sahi A, Sadaoui D, Sadoun N, Djerrada A (2017) Effects of magnetic field on natural convection heat transfer in a T-shaped cavity. Mech Ind 18:407
4. Mojumder S, Sourav S, Sumon S, Mamun M (2015) Combined effect of Reynolds and Grashof numbers on mixed convection in a lid-driven T-shaped cavity filled with water-Al_2O_3 nanofluid. J Hydrodyn Ser B 27:782–794
5. Hatami M, Zhou J, Geng J, Song D, Jing D (2017) Optimization of a lid-driven T-shaped porous cavity to improve the nanofluids mixed convection heat transfer. J Mol Liq 231:620–631
6. Esfe MH, Arani AAA, Yan W-M, Aghaei A (2017) Natural convection in T-shaped cavities filled with water-based suspensions of COOH-functionalized multi walled carbon nanotubes. Int J Mech Sci 121:21–32
7. Almeshaal MA, Kalidasan K, Askri F, Velkennedy R, Alsagri AS, Kolsi L (2019) Three-dimensional analysis on natural convection inside a T-shaped cavity with water-based CNT–aluminum oxide hybrid nanofluid. J Therm Anal Calorim 137:1–10
8. Hussain S, Armaghani T, Jamal M (2019) Magnetoconvection and entropy analysis in T-shaped porous enclosure using finite element method. J Thermophys Heat Transf 33:1–12
9. Izadi M, Oztop HF, Sheremet MA, Mehryan S, Abu-Hamdeh N (2019) Coupled FHD–MHD free convection of a hybrid nanoliquid in an inversed T-shaped enclosure occupied by partitioned porous media. Numer Heat Transf Part A Appl 76:479–498
10. Izadi M, Mohebbi R, Karimi D, Sheremet MA (2018) Numerical simulation of natural convection heat transfer inside a ⊥ shaped cavity filled by a MWCNT-Fe_3O_4/water hybrid nanofluids using LBM. Chem Eng Process Process Intensif 125:56–66
11. Sarkar A, Alim M, Munshi MJH, Ali M (2019) Numerical study on MHD mixed convection in a lid driven cavity with a wavy top wall and rectangular heaters at the bottom. In: AIP conference proceedings, p 030004
12. Ma Y, Mohebbi R, Rashidi M, Yang Z (2019) Mixed convection characteristics in a baffled U-shaped lid-driven cavity in the presence of magnetic field. J Therm Anal Calorim. https://doi.org/10.1007/s10973-019-08900-7
13. Ma Y, Mohebbi R, Rashidi M, Yang Z, Sheremet MA (2019) Numerical study of MHD nanofluid natural convection in a baffled U-shaped enclosure. Int J Heat Mass Transf 130:123–134
14. Ma Y, Mohebbi R, Rashidi MM, Manca O, Yang Z (2019) Numerical investigation of MHD effects on nanofluid heat transfer in a baffled U-shaped enclosure using lattice Boltzmann method. J Therm Anal Calorim 135:3197–3213
15. Selimefendigil F, Öztop HF (2019) MHD mixed convection of nanofluid in a flexible walled inclined lid-driven L-shaped cavity under the effect of internal heat generation. Phys A 534:122144

16. Sheremet MA, Pop I, Ishak A (2017) Time-dependent natural convection of micropolar fluid in a wavy triangular cavity. Int J Heat Mass Transf 105:610–622
17. Ismail HNA, Abourabia AM, Hammad DA, Ahmed NA, El Desouky AA (2019) On the MHD flow and heat transfer of a micropolar fluid in a rectangular duct under the effects of the induced magnetic field and slip boundary conditions. SN Appl Sci 2:25
18. Shafee A, Haq RU, Sheikholeslami M, Herki JAA, Nguyen TK (2019) An entropy generation analysis for MHD water based Fe_3O_4 ferrofluid through a porous semi annulus cavity via CVFEM. Int Commun Heat Mass Transf 108:104295
19. Haq RU, Soomro FA, Öztop HF, Mekkaoui T (2019) Thermal management of water-based carbon nanotubes enclosed in a partially heated triangular cavity with heated cylindrical obstacle. Int J Heat Mass Transf 131:724–736
20. Haq RU, Soomro FA, Hammouch Z, Rehman SU (2018) Heat exchange within the partially heated C-shape cavity filled with the water based SWCNTs. Int J Heat Mass Transf 127:506–514
21. Hamid M, Usman M, Khan Z, Haq R, Wang W (2019) Heat transfer and flow analysis of Casson fluid enclosed in a partially heated trapezoidal cavity. Int Commun Heat Mass Transf 108:104284